Non-Traditional, Safe, High-Voltage Rechargeable Cells of Long Cycle Life

Maria Helena Braga[a,b,*] Chandrasekar M. Subramaniyam [a], Andrew J. Murchison[a], John B. Goodenough[a*]

[a]Materials Science and Engineering Program and Texas Materials Institute,
The University of Texas at Austin, Austin, TX 78712.
[b]LAETA, Engineering Physics Department, FEUP, University of Porto, Portugal.
*Correspondence to: mbraga@fe.up.pt; jgoodenough@mail.utexas.edu

1. Neutron Powder Diffraction:

The high-resolution NPD patterns were refined for a $LiNi_{0.5}Mn_{1.5}O_4$ spinel structure with Fd-3m space group containing a Li-rich Li_2MnO_3 layered phase (C2/m) as shown in Fig. S1. The crystallographic details of the spinel phase are tabulated in Table S1. The refinement results show that the pristine sample consists of 96(11)wt.% spinel phase and the rest is the Li-rich component with C2/m monoclinic space group. Doping with F has a considerable effect on the relative amount of each phase; the weight fraction of spinel phase reduces to 78(3)wt% and that of Li-rich component increases to 22(1) wt.%.

The NPD data were obtained in the 2ϑ angular range 4 to 164° with a step size of 0.125°. GSAS-II was used to perform Rietveld analysis of the obtained NPD data. The refining parameters included background coefficients, zero-shift, peak-shape parameters, lattice parameters, the positional parameters of oxygen, isotropic atomic displacement parameters (U_{iso}), and the occupancy of Mn and Ni.

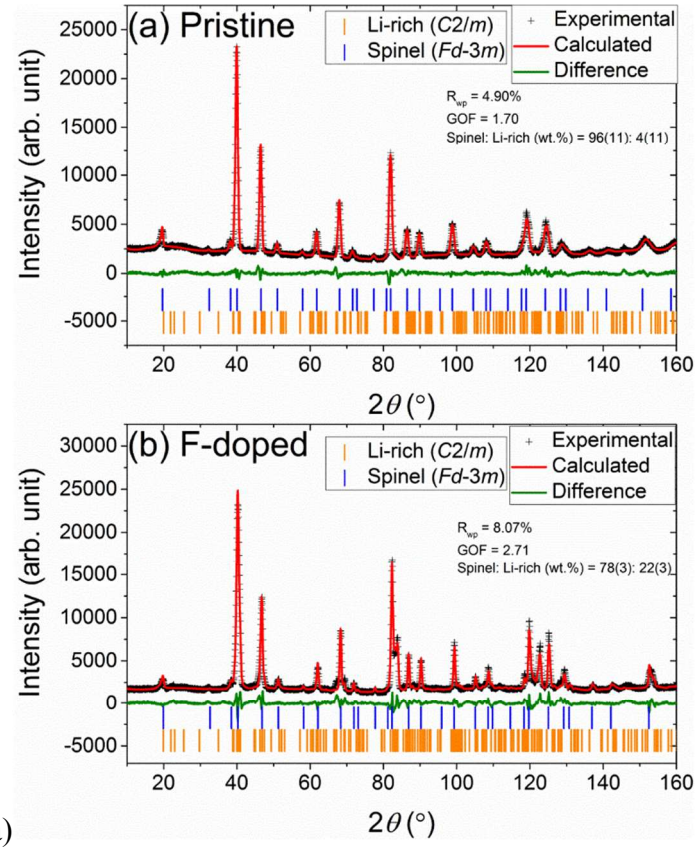

a)

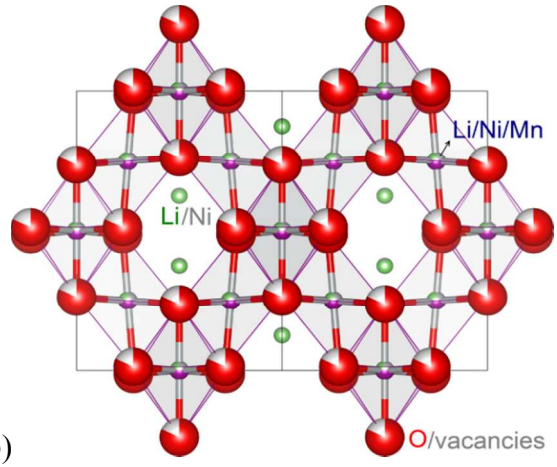

b)

Fig. S1 a) ECHIDNA high-resolution NPD patterns of the spinel phase in the pristine (up) and F-doped (bottom) samples after refinement; b) Refined structure of $(Li_{0.934(2)}Ni_{0.066(2)})(Li_{0.217(21)}Ni_{0.210(3)}Mn_{0.573(19)})_2O_{3.28(8)}$ or $Li_{1.36}Ni_{0.49}Mn_{1.15}O_{3.28}$.

Table S1. Crystallography of the spinel phase in the pristine (up) and F-doped (bottom) samples, obtained from refinement results of the high-resolution NPD collected with ECHIDNA.

Pristine sample Space group: $Fd\bar{3}m$ a = 8.2021(3) Å						
Atoms	Site	x	y	z	U_{iso}	Occupancy
Li	8*a*	1/8	1/8	1/8	0.014(1)*	1
Ni	16*d*	1/2	1/2	1/2	0.014(1)*	0.230(1)#
Mn	16*d*	1/2	1/2	1/2	0.014(1)*	0.770(1)#
O	32*e*	0.26310(5)	0.26310(5)	0.26310(5)	0.014(1)*	1

F-doped sample Space group: $Fd\bar{3}m$ a = 8.1726(3) Å						
Atoms	Site	x	y	z	U_{iso}	Occupancy
Li	8*a*	1/8	1/8	1/8	0.015(1)*	1
Ni	16*d*	1/2	1/2	1/2	0.015(1)*	0.242(2)#
Mn	16*d*	1/2	1/2	1/2	0.015(1)*	0.758(2)#
O	32*e*	0.26327(8)	0.26327(8)	0.26327(8)	0.015(1)*	0.95
F	32*e*	0.26327(8)	0.26327(8)	0.26327(8)	0.015(1)*	0.05

* constrained to be same. # constrained sum to the unity.

2. Additional SEM figures

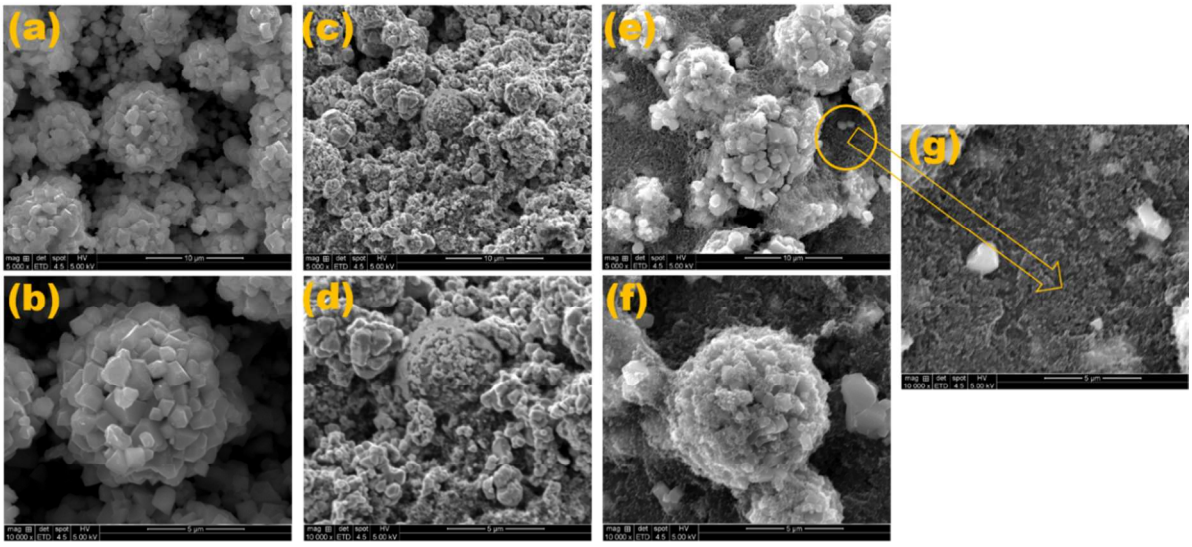

Fig. S2 FESEM of (a-b) pristine F doped LNMO cathode; (c-d) cathode with Super P Carbon (8:1:1) and with PVDF; (e-g) cathode with Super P Carbon (8:1:1), PVDF and covered with SN (7:3). (a), (c) and (e) magnification 5,000x; (b), (d), (f), (g) magnification 10,000x

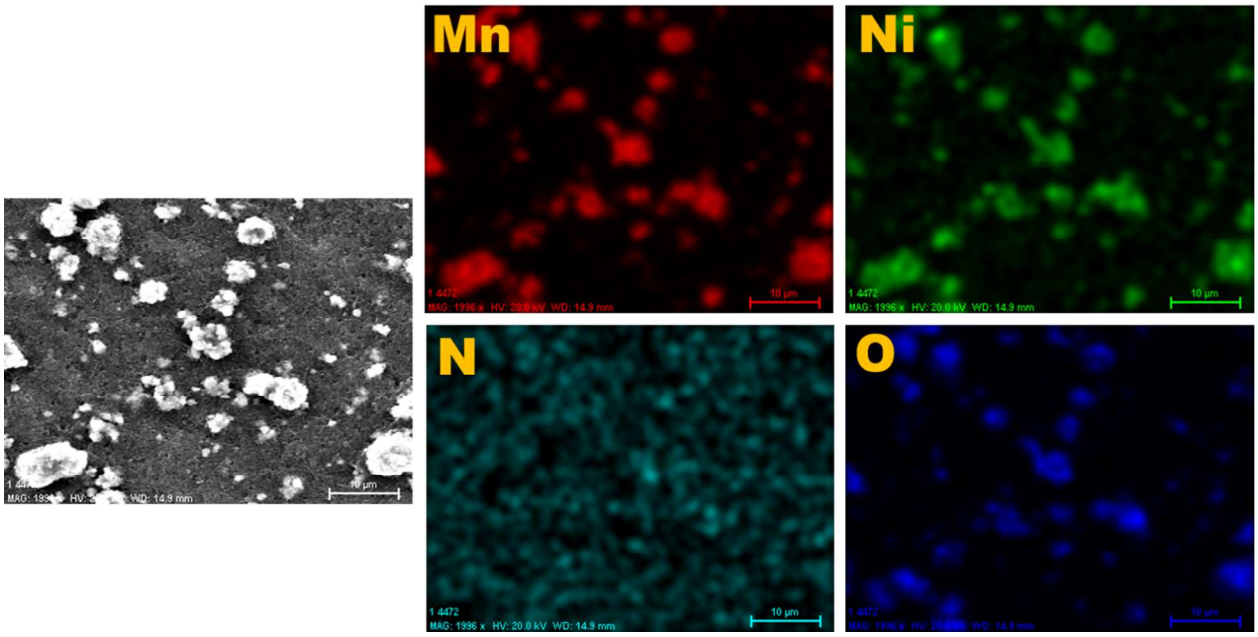

Fig. S3 EDS mapping of cathode electrode of left-hand image containing the active material, PVDF, Super P Carbon (8:1:1) and covered with plasticizer SN (7:3) before cycling. Magnification 20,000x

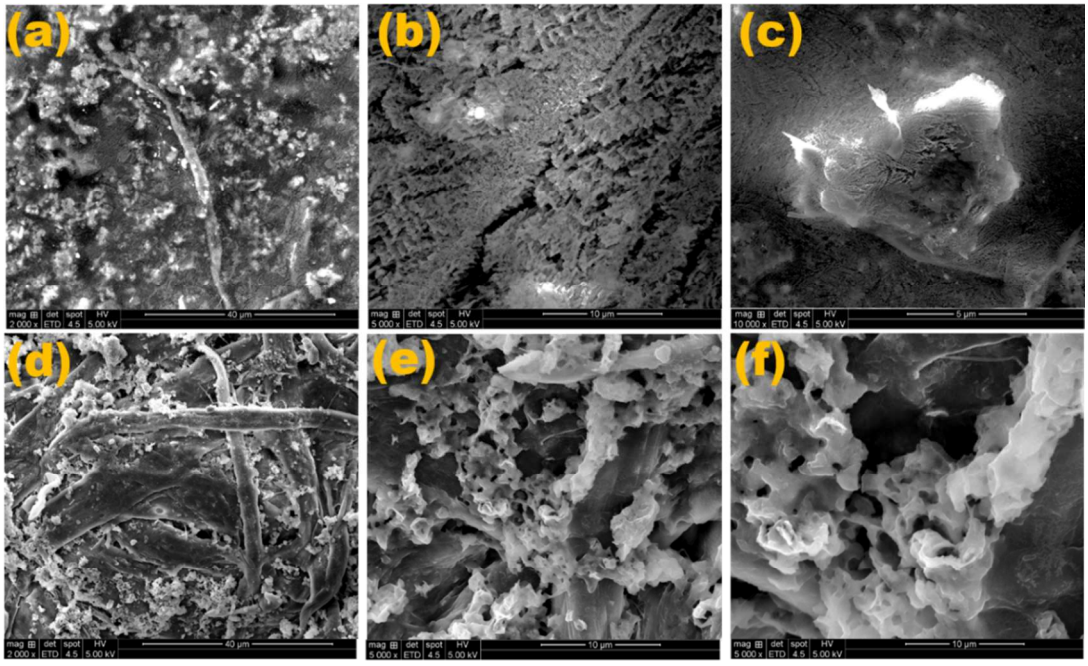

Fig. S4 Ex-situ FESEM after cycling of a cell with (a-c) Cathode with PVDF, Super P Carbon (8:1:1), blended with plasticizer (7:3) with glass electrolyte; (d-f) paper containing glass electrolyte. (a), (d) magnification 2,000x; (b), (e), (f), magnification 5,000x; (c), magnification 10,000x.

3. Additional electrochemical tests

Room temperature electrochemical tests with additional all-solid-state cells are shown in Fig. S5 to S8.

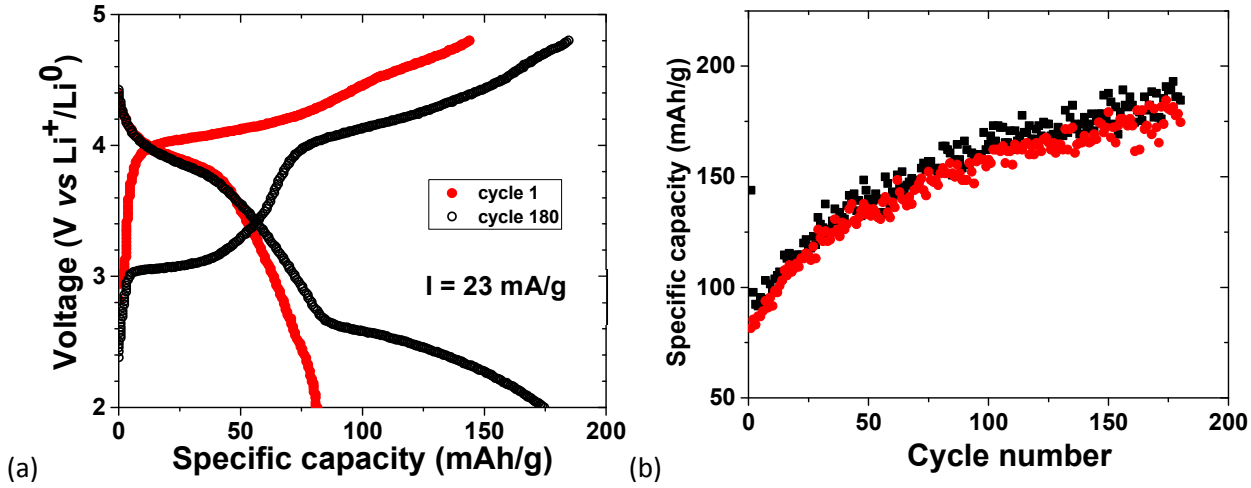

Fig. S5 (a) and (b) Charge/discharge performance of an all-solid state cell assembled as those of Figs. 2,3, and 5. Specific current: 23 mA g^{-1} of active material. Specific capacity and current are given per mass of active cathode material (layered-spinel composite).

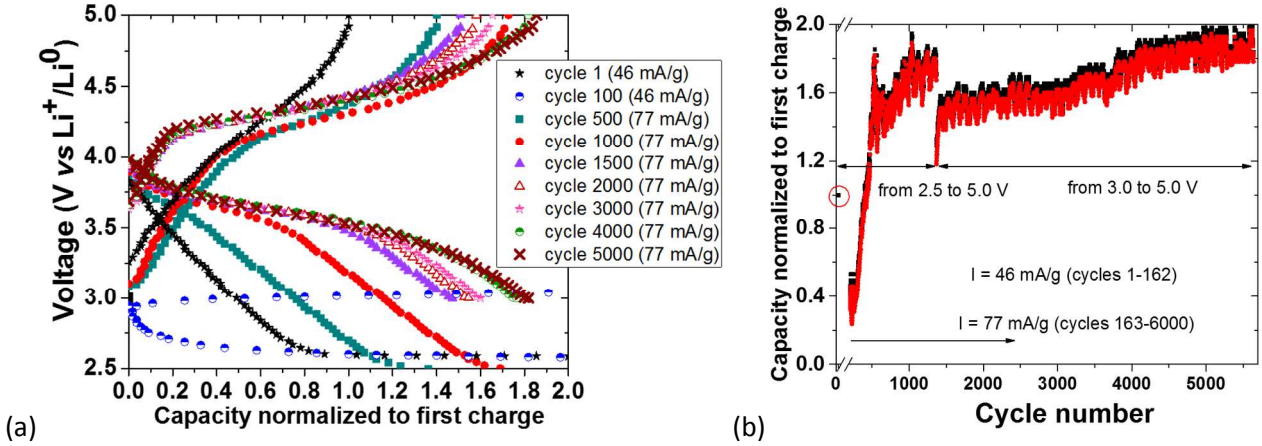

Fig. S6 a) and b) Charge/discharge performance of an all-solid state cell assembled as those of Figs. 2,3, and 5. Specific capacity and currents are given per mass of active cathode material (layered-spinel composite).

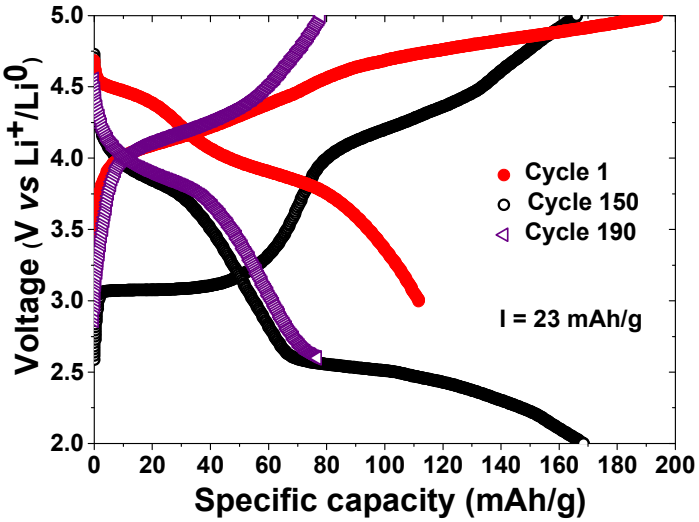

Fig. S7 Cycling of an all-solid state cell assembled the same way as those of Figs. 2,3, and 5. Specific current: 23 mA g^{-1} of active material. Specific capacity and current are given per mass of active cathode material (layered-spinel composite).

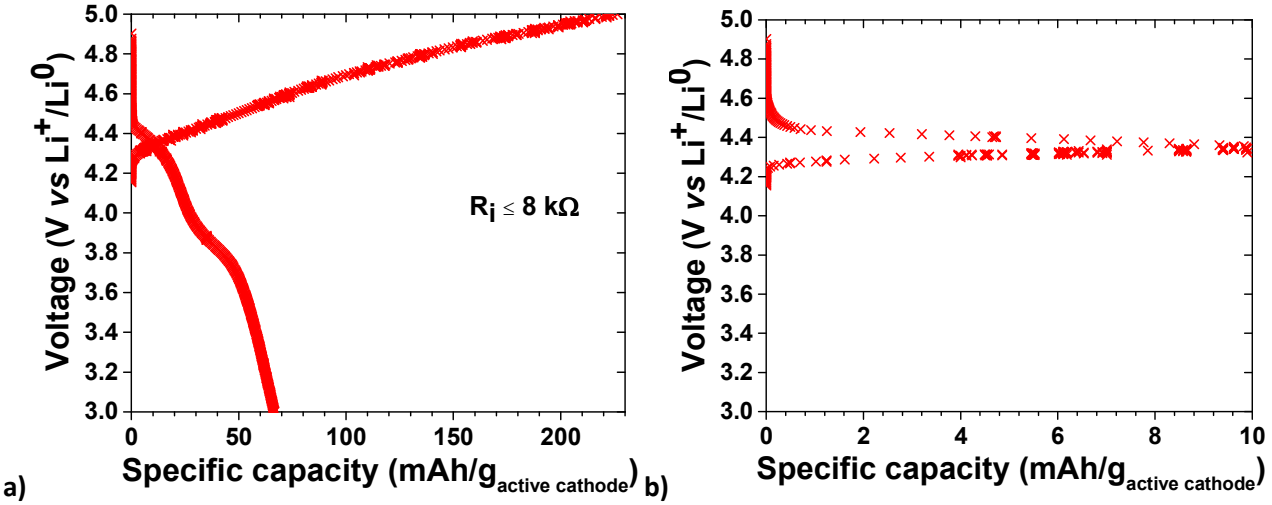

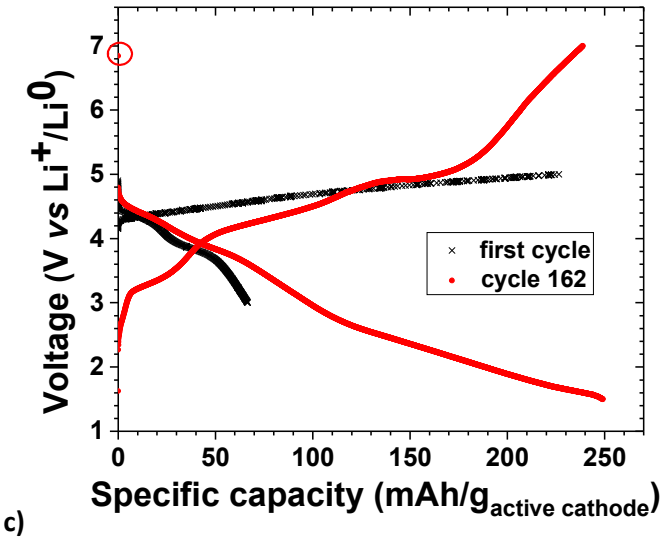

c)

Fig. S8 First cycle of an all-solid state cell assembled the same way as those of Figs. 2, 3, and 5. Specific current: 18 mA g^{-1} of active material. Experiment performed in a Bio-Logic potentiostat. a) full scale; b) zoom c) cycle 1 and 162. In the cycle 162 the cell was charged to 7 V; from 5.2 to 7 V the charge as a capacitor character; on discharge, the data was acquired with a 10 s interval, after the first point. Specific capacity and current are given per mass of active cathode material (layered-spinel composite).

The nature of self-charge.

1. There are two self-charge processes; one is without plating and one is with an anode plating. The first and more common happens in almost all kinds of battery cells (if anode and cathode show an open circuit voltage different from zero) especially in "charged cells" that are not charged prior to discharge (e.g. primary cells). This phenomenon of self-charge does not involve plating of an anode, it happens due to the necessity to align each electrode's Fermi level with the electrolyte's Fermi level in contact with the electrodes at the electrode/electrolyte interface as demonstrated in ref. [S1]. The anode is at a higher Fermi level than that of the electrolyte and cathode. To align the higher Fermi level of the anode with the lower Fermi level of the electrolyte, an Electrical Double Layer Capacitor (EDLC) is formed at the interface in a way that the potential (energy per unit charge) increases in the direction of the electrolyte (Fig. S9). Therefore, the electric field has to pointing the direction of the anode and hence the free electrons that accumulate at the surface of the anode at the anode/electrolyte interface and the mobile cations in the electrolyte form an EDLC. On the cathode side, the electric field has to point towards the electrolyte and electron deficiencies holes on the cathode side form an EDLC with cation deficiencies in the electrolyte.
2. The second self-charge phenomenon is characteristic of the present electrolyte containing both ions and dipoles; it involves a plating of an anode from the working cation of the electrolyte; as shown in the paper, we argue that this self-charge is the result of

equalization of the Fermi levels across the negative-electrode/electrolyte interface and a time lag between the arrival at the interface of the fast-moving electrolyte cation and the slower-moving electrolyte electric dipoles. Equalization of the Fermi levels by the interface EDLC (Fig. S9) is retained on arrival of the electric-dipole charge by a plating of an electrolyte cation onto the negative electrode, i.e. a *self-charge*, that creates a negative charge in the electrolyte.

3. **Self-charge due to alignment of the dipoles.**

According to Gauss's law, the electric field outside a parallel plate capacitor (EDLCs) is zero. Therefore, the fields ***E'*** and ***E''*** of Fig. S10 must sum to zero in the bulk electrolyte when no dipoles are aligned. The alignment of the dipoles leading to a uniform array is equivalent to a surface charge. The electric field ***E'''*** resulting from the alignment of the electric dipoles inside the electrolyte must be compensated by the surface charge in the electrolyte/electrode EDLCs. The surface charge increment results in a higher ***E''*** that then compensates ***E'''*** and ***E'*** in the electrolyte.

At the EDLCs $Q_i = C_i \Delta V$ where Q_i; is the initial capacity, C_i the initial capacitance, and ΔV the potential difference ($\Delta\phi_{EDLC}$) the accumulation of extra charge cannot result in the increase of the potentials $\Delta\phi_{EDLC}$ (Fig. S9) since they are fixed due to the equalization of the Fermi levels at each given charge or discharge time. Therefore, $C_i = \varepsilon_0 \frac{A}{d_i}$ has to increase by decreasing d_i. The thickness of an EDLC is $0.3\ \mathrm{nm} \leq d_i \leq 0.8\ \mathrm{nm}$, which does not allow for the necessary increase in C_i; but decreasing d_i will increase exponentially the electron tunneling probability (see ref. [S1]) and the extra capacity ΔQ can then be plated leaving behind negative charges (Li^+- deficiencies) at the anode side of the electrolyte. Moreover since plating creates negative charge in the electrolyte on the anode side, the electric field in the direction of ***E'''*** increases again and more cations are attracted to the anode surface while the cation-deficiencies diffuse towards the cathode charging the electrolyte/plasticizer EDLC. Furthermore, charging the electrolyte negatively makes the Fermi level of the electrolyte increase, discharging the anode/electrolyte EDLC and charging the electrolyte/plasticizer EDLC, which will discharge during cell's discharge and contribute with the corresponding extra capacity. In Fig. 4 it can be observed that the increase in charge capacity is proportional to the discharge capacity, even after the theoretical capacity of active material in the cathode is surpassed.

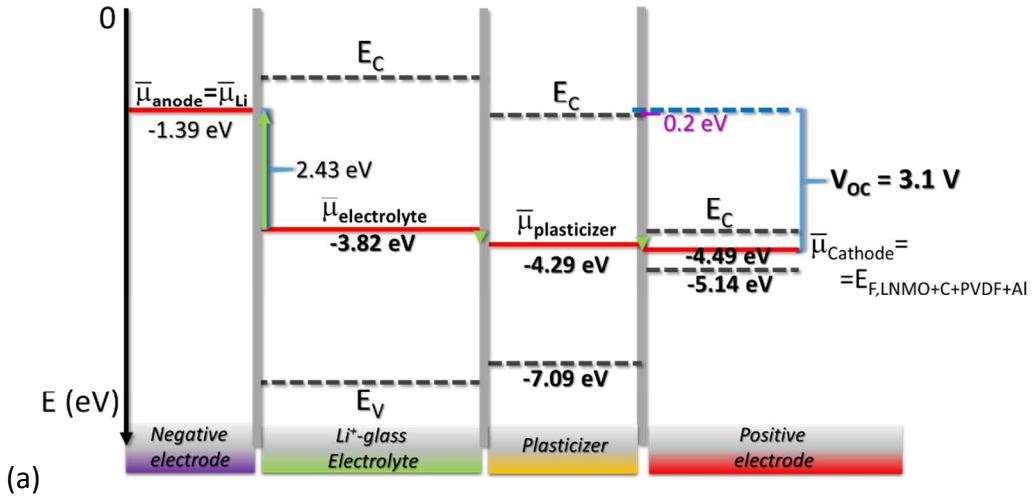
0
E_C
$\bar{\mu}_{anode}=\bar{\mu}_{Li}$
-1.39 eV
2.43 eV
$\bar{\mu}_{electrolyte}$
-3.82 eV
E_C
0.2 eV
V_{OC} = 3.1 V
$\bar{\mu}_{plasticizer}$
-4.29 eV
E_C
-4.49 eV
-5.14 eV
$\bar{\mu}_{Cathode}$=
=$E_{F,LNMO+C+PVDF+Al}$
-7.09 eV
E_V
E (eV)
Negative electrode
Li+-glass Electrolyte
Plasticizer
Positive electrode

(a)

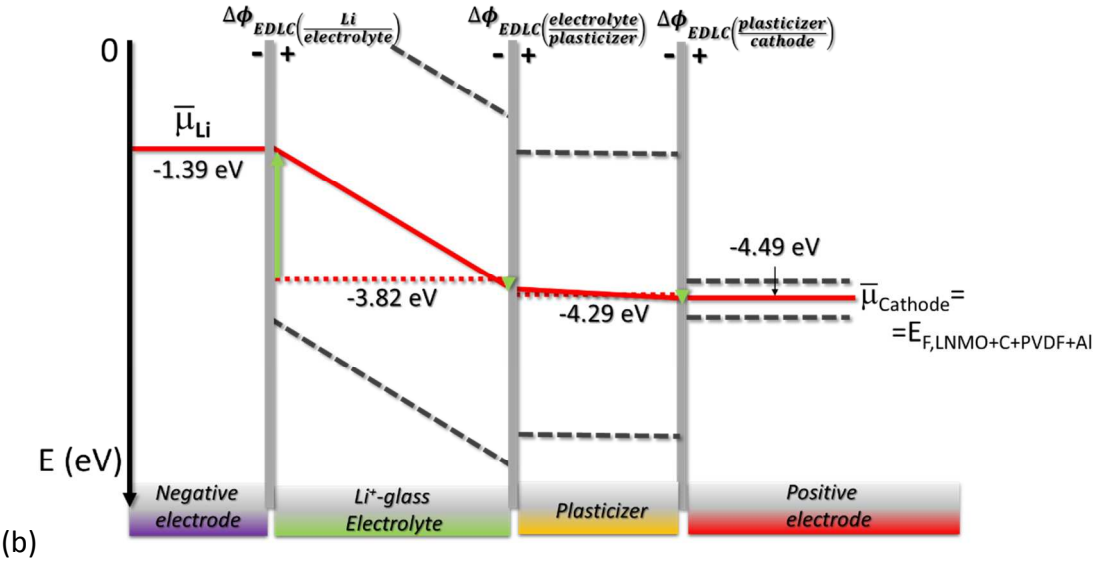
$\Delta\phi_{EDLC}\left(\frac{Li}{electrolyte}\right)$
$\Delta\phi_{EDLC}\left(\frac{electrolyte}{plasticizer}\right)$
$\Delta\phi_{EDLC}\left(\frac{plasticizer}{cathode}\right)$
0
$\bar{\mu}_{Li}$
-1.39 eV
-3.82 eV
-4.29 eV
-4.49 eV
$\bar{\mu}_{Cathode}$=
=$E_{F,LNMO+C+PVDF+Al}$
E (eV)
Negative electrode
Li+-glass Electrolyte
Plasticizer
Positive electrode

(b)

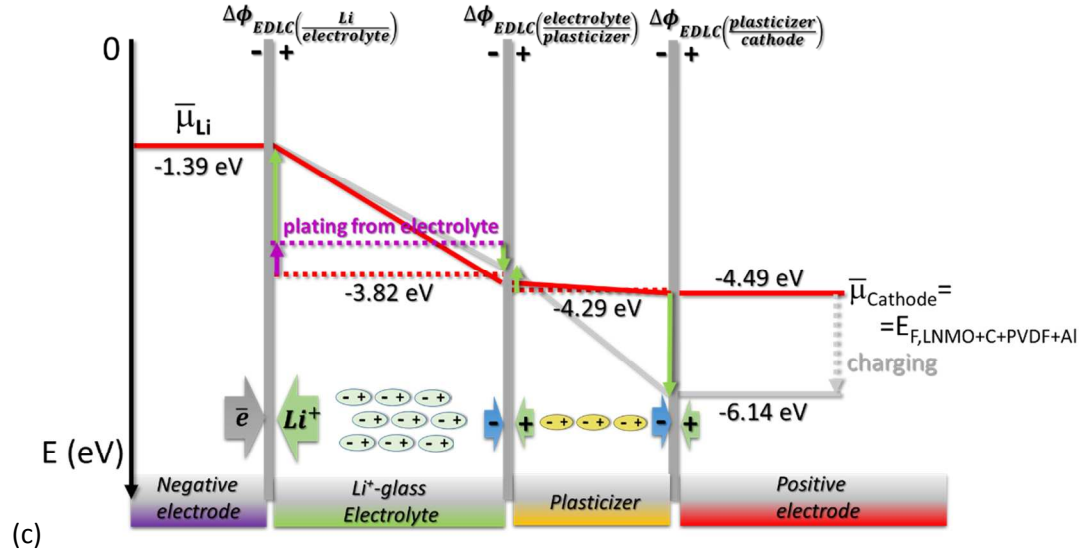
$\Delta\phi_{EDLC}\left(\frac{Li}{electrolyte}\right)$
$\Delta\phi_{EDLC}\left(\frac{electrolyte}{plasticizer}\right)$
$\Delta\phi_{EDLC}\left(\frac{plasticizer}{cathode}\right)$
0
$\bar{\mu}_{Li}$
-1.39 eV
plating from electrolyte
-3.82 eV
-4.29 eV
-4.49 eV
$\bar{\mu}_{Cathode}$=
=$E_{F,LNMO+C+PVDF+Al}$
charging
-6.14 eV
$\bar{e}$
Li^+
E (eV)
Negative electrode
Li+-glass Electrolyte
Plasticizer
Positive electrode

(c)

Fig. S9 Schematics showing the electrochemical potentials of the species in contact in the electrochemical cells. (a) before alignments; (b) aligned at open-circuit voltage; (c) aligned at open-circuit in comparison with alignment when charged and plating from the electrolyte occurred.

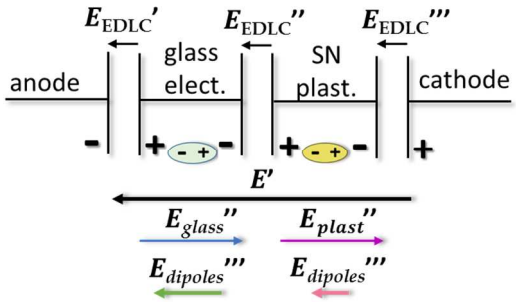

Fig. S10 Schematics showing the electric fields and double layer capacitors inside the electrochemical/electrostatic cell.

References

[S1] Braga, M.H., Grundish, N.S., Murchison, A.J., and Goodenough, J.B. "Reply to comment on Alternative Strategy for a Safe Rechargeable Battery" submitted (2017).